ChemInform Abstract: Synthesis and Structure of the Gibbsite Intercalation Compounds (LiAl2(OH)6)X (X: Cl, Br, NO3) and (LiAl2(OH)6)Cl×H2O Using Synchrotron X-Ray and Neutron Powd…

ARTICLE *in* CHEMINFORM · APRIL 2010

Impact Factor: 0.74 · DOI: 10.1002/chin.199715015

Synthesis and Structure of the Gibbsite Intercalation Compounds $[LiAl_2(OH)_6]X$ {X = Cl, Br, NO_3} and $[LiAl_2(OH)_6]Cl{\cdot}H_2O$ Using Synchrotron X-ray and Neutron Powder Diffraction

A. V. Besserguenev, A. M. Fogg, R. J. Francis, S. J. Price, and D. O'Hare*,†

Inorganic Chemistry Laboratory, University of Oxford, South Parks Road, Oxford, UK OX1 3QR

V. P. Isupov and B. P. Tolochko

Institute of Solid State Chemistry, Siberian Branch of Russian Academy of Science, Kutateladze 18, Novosibirsk 630128, Russia

Received May 31, 1996. Revised Manuscript Received September 4, 1996[⊗]

Treatment of gibbsite {γ-$Al(OH)_3$} with the lithium salts LiX {X = Cl, Br, NO_3} in water leads to intercalation of both the cations and anions into the host structure to give $[LiAl_2(OH)_6]X{\cdot}H_2O$ {X = Cl, Br, NO_3}. Thermogravimetric analysis indicates that these materials can be readily dehydrated to give highly hydroscopic, crystalline layered phases $[LiAl_2(OH)_6]X$ {X = Cl, Br, NO_3}. The structures of these dehydrated phases have been determined by synchrotron X-ray and neutron powder diffraction. The dehydrated intercalates with {X = Cl, Br} are isomorphous and crystallize in the $P6_3/mcm$ space group. $[LiAl_2(OH)_6]NO_3$ adopts a similar structure but crystallizes in space group $P6_3/m$ due to disorder of the intercalated nitrate anions in the crystallographic *ab* plane. All the intercalates consist of eclipsed $Al(OH)_3$ layers stacked along the *c*-axis with the halide or nitrate ions located at the cell edges and midway between the $Al(OH)_3$ layers. The lithium ions have been located in the unfilled octahedral sites within the $Al(OH)_3$ layers. The structure of the hydrated phase $[LiAl_2(OH)_6]Cl{\cdot}H_2O$ has also been determined, it adopts a similar structure with eclipsed $[LiAl_2(OH)_6]^+$ layers stacking along the *c*-axis. However the intercalated Cl^- ions and water molecules were found to be disordered over five sites located midway between the $Al(OH)_3$ layers.

Introduction

Intercalation of inorganic or organic ions into lamellar inorganic matrixes is now a widely studied reaction.[1−3] It provides synthetic chemists with a low-temperature route to modify both the structural characteristics and also the reactivity of inorganic solids in a subtle and controllable manner.[4,5] Aluminum hydroxide, $Al(OH)_3$, exists as three structural modifications: gibbsite, bayerite, and nordstrandite.[6−9] The structure of naturally occurring gibbsite was first reported in 1933 and then later reinvestigated in 1973.[9] It adopts a layered structure as shown in Figure 1. Each of the $Al(OH)_3$ layers consists of nearly close packed OH^- ions in which the Al^{3+} ions occupy two-thirds of the octahedral holes. Consequently, the structure has pseudohexagonal symmetry but small distortions of the OH^- ions lead to a small shift of the adjacent layers and a lowering of the crystal symmetry to monoclinic.

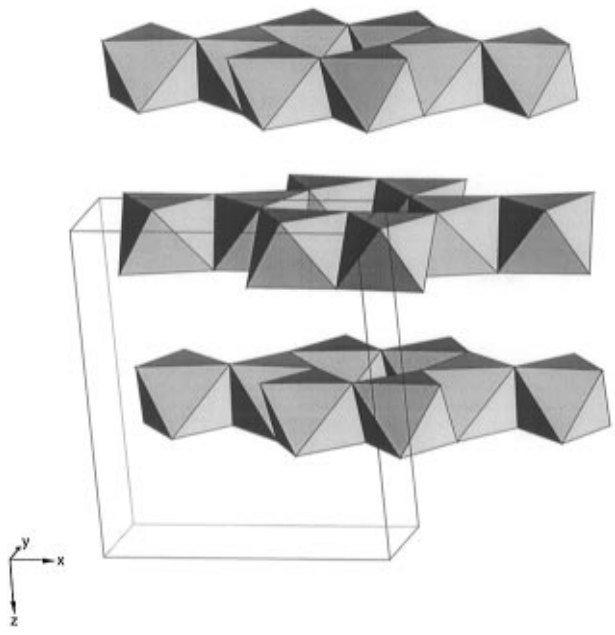

Figure 1. Structure of gibbsite (γ-$Al(OH)_3$).

† Royal Society of Chemistry Sir Edward Frankland Fellow.

⊗ Abstract published in *Advance ACS Abstracts,* December 15, 1996.

(1) Schollhorn, R. *In Intercalation Compounds*; Atwood, J. L., Davies, J. E. D., MacNicol, D. D., Eds.; Academic Press: London, 1984; pp 249−334.
(2) O'Hare, D. *In Inorganic Materials*; Bruce, D. W., O'Hare, D., Eds.; J. Wiley and Sons: London, 1996.
(3) Jacobson, A. J. *In Solid State Chemistry Compounds;* Cheetham, A. K., Day, P., Eds.; Clarendon Press: Oxford, 1992; p 304.
(4) Pinnavaia, T. J. *Science* **1983**, *220*, 365.
(5) Schollhorn, R. *In Chemical Reactions in Organic and Inorganic Constrained Systems*; Setton, R., Ed.; D. Reidel Publishing Co.: New York, 1986; Vol. 165, pp 323−340.
(6) Zigan, F.; Joswig, W.; Burger, N. *Z. Kristallogr.* **1978**, *148*, 255−273.
(7) Megaw, H. D. *Z. Kristallogr.* **1933**, *87*, 185−204.
(8) Bosmans, H. J. *Acta. Crystallogr.* **1970**, *B26*, 649−652.
(9) Saalfeld, H.; Wedde, M. *Z. Kristallogr.* **1974**, *139*, 129−135.

S0897-4756(96)00316-X CCC: $14.00 Published 1997 by the American Chemical Society

Gibbsite [γ-$Al(OH)_3$] has found applications as a flame retardant, paper additive, and a feedstock in the production of aluminum via the Bayer process.[10−13] In fact, the crystallization of gibbsite using the Bayer process involves key organic species which direct the crystallization, it is thought that intercalation processes could be involved in some of the key steps.[11] Therefore an understanding of the basic intercalation chemistry of gibbsite would be of considerable interest.

Experimental Section

Synthesis. Intercalation was achieved by stirring a suspension of the gibbsite[14] (ca. 0.6 g) in an aqueous solution containing a 4-fold molar excess of lithium salts (LiCl, LiBr or $LiNO_3$) at 90 °C for 6 h. Samples were washed with 5 × 10 mL of deionized water and dried in a oven at 90 °C or 1−2 h to give samples of idealized composition $[LiAl_2(OH)_6]X{\cdot}yH_2O$ {X = Cl; Br; NO_3}. Elemental Anal. Found (Calcd) for $Al(OH)_3(LiCl)_{0.57}(H_2O)_{0.87}$: Al 22.23 (22.84); Li 3.15 (3.38); Cl 17.28 (17.25); H 4.05 (4.05). Found (Calcd) for $Al(OH)_3(LiBr)_{0.57}(H_2O)_{0.73}$: Al 18.89 (19.14); Li 2.58 (2.83); Br 35.18 (32.58); H 3.16 (3.18). Found (Calcd) for $Al(OH)_3(LiNO_3)_{0.50}(H_2O)_{0.8}$: Al 18.89 (20.98); Li 2.62 (2.83); N 4.93 (5.72); H 3.34 (3.60). The dehydrated phases of idealized composition $[LiAl_2(OH)_6]X$ {X = Cl (**1**); Br (**2**); NO_3; (**3**)} were prepared by heating in a dynamic vacuum for 6 h at 140 °C for **1** and 170 °C for **2** and **3**, respectively. These samples were extremely hydroscopic, and all manipulations were carried in an inert-atmosphere drybox.

Measurements. Powder X-ray patterns were recorded either on a Siemens D5000 diffractometer equipped with a linear position-sensitive detector using Cu $K\alpha_1$ radiation in transmission geometry on samples sealed in 0.3 mm capillaries or in transmission mode on Station 2.3 at the SRS Daresbury Laboratory. For powder neutron diffraction data ca. 3 g samples were sealed in a vanadium can under dry nitrogen and data collected on the POLARIS diffractometer at the UK spallation neutron source ISIS, Rutherford Appleton Laboratory, UK. Powder refinements used the data measured in the C-bank (back scattering) over the time-of-flight range 2−18 ms. Initial trial structure solutions and diffractograms were generated within the INSIGHTII package from MSI.[15] Final structure refinements were performed using the GSAS suite.[16] The GSAS suite has the ability to refine a model simultaneously against several data sets specifically in the case of **1** for synchrotron X-ray and time-of-flight powder neutron data. In the refinements of all the samples we encountered problems with refinement of the isotropic temperatures. Consequently, we were forced to equivalence all the isotropic temperature factors and use one overall parameter. TGA measurements were performed on a STA-1500, using a heating rate of 5 °C/min between 25 and 400 °C under static air.

Results and Discussion

Poeppelmeier and co-workers[17] have investigated the solid-state room-temperature reaction of lithium hydroxide with bayerite under flowing water-saturated nitrogen gas to give lithium dialuminate $LiAl_2(OH)_7{\cdot}2H_2O$. Rietveld refinement of X-ray and neutron powder diffraction patterns indicate that the structure is composed of $[LiAl_2(OH)_6]^+$ layers separated by water molecules and hydroxide ions. This material is closely related to the hydrotalcite minerals which have general formula $[(M^{2+})_{1-x}(M^{3+})_x(OH)_2]^{x+}(A^{m-})_{x/m}{\cdot}nH_2O$, where M^{2+} = Mg, Ni, Fe; M^{3+} = Al, Cr; A = OH^-, Cl^-, CO_3^{2-}.[18−25] A wide range of inorganic anions may be exchanged into hydrotalcite minerals, and preferential intercalation of inorganic ions has been reported.[26,27]

Intercalation of gibbsite by the lithium salts (LiX; X = Cl^-, Br^-, and NO_3^-) in water can be readily achieved by addition of an excess of the lithium salts to a suspension of gibbsite in water and then heating to 90 °C for 6 h. The mechanism of intercalation in these systems is still not clear, but in situ XRD measurements[28] give no evidence for staging intermediates or a solution/nucleation route as suggested for intercalation in MPX_3 materials.[29] The intercalates can be isolated by filtration, after washing to remove any unreacted lithium salts and drying at room temperature. Elemental microanalysis indicates that all these materials have the chemical composition $[LiAl_2(OH)_6]X{\cdot}yH_2O$ {X = Cl, Br, NO_3}. The hydrated forms of some of these compounds have been briefly reported previously, but their structures have not been determined.[30] Thermogravimetric analysis of these hydrated phases indicate that they readily lose water on heating. Figure 2 shows the weight loss and heat flow on heating a sample of $[LiAl_2(OH)_6]Cl{\cdot}H_2O$ between 20−450 °C. On heating to 130 °C, $[LiAl_2(OH)_6]Cl{\cdot}H_2O$ loses 8.91% of its original weight. This weight change corresponds to loss of one water per formula unit to give $[LiAl_2(OH)_6]Cl$ (**1**). No further change is observed until 300 °C, when further weight loss is observed corresponding to the thermal decomposition of the $Al(OH)_3$ layers and formation of condensed material with an idealized chemical composition corresponding to Al_2O_3LiCl. The Al_2O_3LiCl was insufficiently crystalline for structural studies. $[LiAl_2(OH)_6]Br{\cdot}H_2O$ and $[LiAl_2(OH)_6]NO_3{\cdot}H_2O$ exhibit similar thermal stability. The lithium bromide intercalate of gibbsite, $[LiAl_2(OH)_6]Br{\cdot}H_2O$ loses 5.95% of it original weight on heating to 300 °C to give $[LiAl_2(OH)_6]Br$ (**2**); decomposition of the $Al(OH)_3$ layers begins at 340 °C. Whereas $[LiAl_2(OH)_6]NO_3{\cdot}H_2O$ loses 8.6% of it original weight on heating to 225 °C yielding $[LiAl_2(OH)_6]NO_3$ (**3**); the host lattice decomposition begins at 300 °C.

We were particularly interested in the dehydrated materials formed on heating compounds $[LiAl_2(OH)_6]X$ {X = Cl, Br, NO_3} to just below 200 °C. Preliminary XRD measurements showed that these were highly crystalline materials, and so we were prompted to

(10) Friederich, R. O.; Oeberg, N. *J. Met.* **1985**, *37*, 2.
(11) Lectard, A.; Nicolas, F. *J. Met.* **1982**, *35*, 34.
(12) Mahi, P. *Chem. Ind.* **1988**, 445−451.
(13) Ruvalcaba, J. M.; Vargas, O. A.; Cuesta, J. R.; Juarez, H.; Anguiano, P. L. *Bull. Soc. Chillena. Quim.* **1995**, *40*, 421−426.
(14) Sato, T. *J. Appl. Chem.* **1964**, *14*, 303.
(15) INSIGHTII, Molecular Simulations Inc.: San Diego, CA, 1994.
(16) Larson, A. C.; Von Dreele, R. B. *GSAS Reference*, Los Alamos National Laboratory, 1987.
(17) Thiel, J. P.; Chiang, C. K.; Poeppelmeier, K. R. *Chem. Mater.* **1993**, *5*, 297−304.
(18) Serna, C. J.; Rendon, J. L.; Iglesias, J. E. *Clays Clay Miner.* **1982**, *30 N3*, 180−184.
(19) Meyn, M.; Beneke, K.; Lagaly, G. *Inorg. Chem.* **1990**, *29*, 5201−5207.
(20) Chisem, I. C.; Jones, W. *J. Mater. Chem.* **1994**, *4*, 1737−1744.
(21) Sisssoko, I.; Iyagba, E. T.; Biloen, P. *J. Solid State Chem.* **1985**, *60*, 283−288.
(22) Dutta, P. K.; Puri, M. *J. Phys. Chem.* **1988**, *93*, 376−381.
(23) Nemudry, A. P.; Isupov, V. P.; Kotsupalo, N. P.; Boldyrev, V. V. *React. Solids* **1986**, *1*, 221−226.
(24) Chibwe, K.; Jones, W. *J. Chem. Soc., Chem Commun.* **1989**, 926−927.
(25) Cooper, S.; Dutta, P. K. *J. Phys. Chem.* **1990**, *94*, 114−118.
(26) Miyata, S.; Hirose, T. *Clays Clay Miner.* **1978**, *26*, 441.
(27) Miyata, S. *Clays Clay Miner.* **1983**, *31*, 305.
(28) O'Hare, D.; Fogg, A. Unpublished results, 1996.
(29) Clement, R.; Garnier, O.; Jegoudez, J. *Inorg. Chem.* **1986**, *25*, 1404−1409.
(30) Poeppelmeier, K. R.; Hwu, S.-J. *Inorg Chem.* **1987**, *26*, 3297.

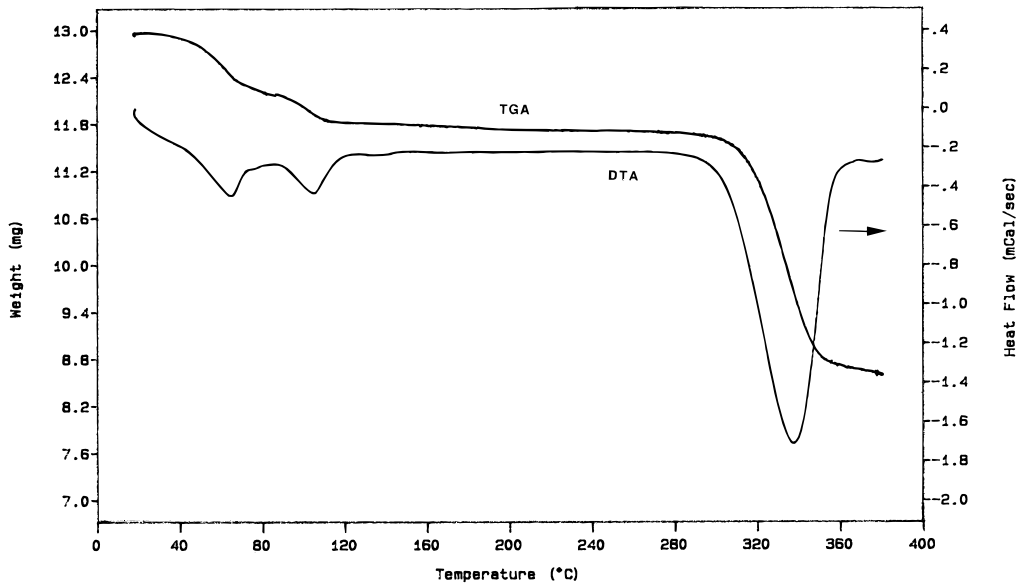

Figure 2. TGA and DTA curves for **4** on heating in air; ramp rate 5 K min^{-1}.

attempt structure determinations using powder diffraction methods. Bulk samples of $[LiAl_2(OH)_6]X$ {X = Cl (**1**), Br (**2**), NO_3 (**3**)} could be readily obtained by heating either $[LiAl_2(OH)_6]X{\cdot}H_2O$, {X = Cl, Br, NO_3} under a dynamic vacuum at 90 °C for 1−2 h. Compounds **1**−**3** are extremely hydroscopic and samples left on the TGA regained all the original weight lost approximately 20 min after cooling to room temperature.

Crystal Structure Determinations. Powder X-ray diffraction indicated that the dehydrated intercalation compounds (**1**−**3**) give significantly higher quality powder diffraction patterns, and so these materials were chosen for initial structural investigation. Synchrotron X-ray and neutron powder diffractograms were recorded for **1** at room temperature. Both diffractograms were indexed using the TREOR program[31] to give a primitive hexagonal cell with approximate dimensions $a = 5.1$ and $c = 14.3$ Å. All the observed reflections in the X-ray and neutron patterns could be indexed on this cell. A systematic absence for the 00*l* reflections ($l = 2n + 1$) was observed, which was consistent with 11 possible hexagonal space groups.

The structure was solved by constructing a number of initial trial solutions based upon stacking of $Al(OH)_3$ layers along the *c*-axis within the INSIGHTII software package.[15] Eventually, we found that a good agreement between the observed and calculated X-ray powder pattern was produced when the unit cell contained two eclipsed $Al(OH)_3$ layers, separated by 7.15 Å. This arrangement of $Al(OH)_3$ layers could be generated in the hexagonal space groups $P6_3$, $P6_3/m$, or $P6_3/mcm$ by placing the Al on the special position $^1/_3$, $^2/_3$, 0. The chloride ion position was again initially found by trying a number of possible sites midway between the $Al(OH)_3$ layers. The best agreement between the observed and calculated X-ray diffraction pattern was found when the Cl^- ions were placed on the edge of the unit cell and midway between the $Al(OH)_3$ layers.

The location and refinement of the Li, H, and O positions was largely based on the powder neutron diffraction data. The location of the lithium ion in these structures has been the subject of much debate in the literature. Some authors have located the Li ions in a tetrahedral position below the aluminum layer;[23] other authors have located them in the octahedral site in the $Al(OH)_3$ layers.[17,18,21] In fact the difference between tetrahedral and octahedral sites is a shift along the *c*-axis. The neutron data clearly show that in these materials the lithium ions were located in the remaining one-third of the octahedral holes within the $Al(OH)_3$ layers which are not filled by Al^{3+} ions. This is in agreement with the location of the lithium ions found by Poeppelmeier in $[LiAl_2(OH)_6]OH{\cdot}2H_2O$.[17]

After location of all the non-hydrogen atoms, the structure was refined using the Rietveld method. The GSAS program suite allowed us to simultaneously use both the synchrotron X-ray and neutron diffraction data. Refinements in both the space groups $P6_3/m$ and $P6_3/mcm$ were carried out. For both space groups the Al, Li, and Cl occupy special positions and so their positional parameters could not be refined; however the oxygen *x* and *y* coordinates are independent variables in $P6_3/m$ but are linked in $P6_3/mcm$. We obtained a slightly better agreement in the space group $P6_3/mcm$. In the final stages of the refinements we noted that the peak shapes of the 00*l* and the *hk*0 reflections were not being equally fitted by the pseudo-Voight peak-shape function. This is possibly not surprising given the lamellar nature of the samples. Therefore in the final cycles of refinement we included additional ansiotropic broadening term to allow for some anisotropic strain or stacking fault disorder. An overall isotropic thermal parameter, $B = 0.301(3)$ Å^2 was used. The final refinement therefore consisted of 44 parameters, with 3585 data points (745 reflections) for the neutron data and 6990 points (81 reflections) for the X-ray data. Final convergence was achieved at $\chi^2 = 6.38$, $R_{wp} = 1.60$ (neutron), $R_{wp} = 10.52\%$ (X-ray), and $R_{wp} = 2.13\%$ (combined datasets). Plots of the final Rietveld fits are given in Figure 3. We also note that the intensity of the strong low angle ($2\theta = 12.04°$) peak is overcalculated; we attribute this discrepancy to there being slighly less sample in the beam at this low angle.

(31) Werner, P.-E.; Eriksson, L.; Westdahl, M. *J. Appl. Crystallogr.* **1985**, *18*, 360.

Table 1. Summary of the Crystallographic Data for Compounds 1−4

	1	2	3	4
empirical formula	$[LiAl_2(OH)_6]Cl$	$[LiAl_2(OH)_6]Br$	$[LiAl_2(OH)_6]NO_3$	$[LiAl_2(OH)_6]Cl{\cdot}H_2O$
formula mass	198.40	242.85	218.90	216.42
crystal system	hexagonal	hexagonal	hexagonal	hexagonal
a, Å	5.10005(8)	5.0996(1)	5.10917(8)	5.0963(3)
c, Å	14.2994(3)	14.9461(6)	14.3738(3)	15.2919(9)
V, Å^3	322.104(9)	336.62(2)	324.940(9)	343.96(3)
space group	$P6_3/mcm$	$P6_3/mcm$	$P6_3/m$	$P6_3/m$
instrument	Station 2.3 (SRS), POLARIS, Bank C	Siemens D5000	Siemens D5000	POLARIS, Bank C
radiation	synchrotron X-rays, TOF neutrons	X-rays, Cu Kα	X-rays, Cu Kα	TOF neutrons
λ, Å	1.5000 (X-ray), TOF(neutron)	1.540 56	1.540 56	TOF (neutron)
ρ_{calc}, g/cm^3	2.05	2.40	2.24	2.11
zero point, deg	0.0006 (X-ray) 2.68 μs (neutron)	0.0032	0.0052	2.68 μs
absorption, A_h	not applied	−0.0086	−0.0020	not applied
preferred orientation, R_0	1.08 (X-ray) 0.94 (neutron)	0.92	0.86	not refined
data points	6990 (X-ray), 3685 (neutron)	3101	4100	3585
reflections fitted	81 (X-ray), 745 (neutron)	37	104	291
parameters refined	44	29	32	51
χ^2	6.36	6.18	5.99	5.27
R_{wp}, %	10.52 (X-ray), 1.60 (neutron), 2.13 (combined)	6.39	6.77	1.26
R_p, %	8.18 (X-ray), 1.96 (neutron), 7.29 (combined)	4.67	5.36	1.31
R_w(expected), %	5.05 (X-ray), 0.5 (neuton)	2.57	2.77	0.55

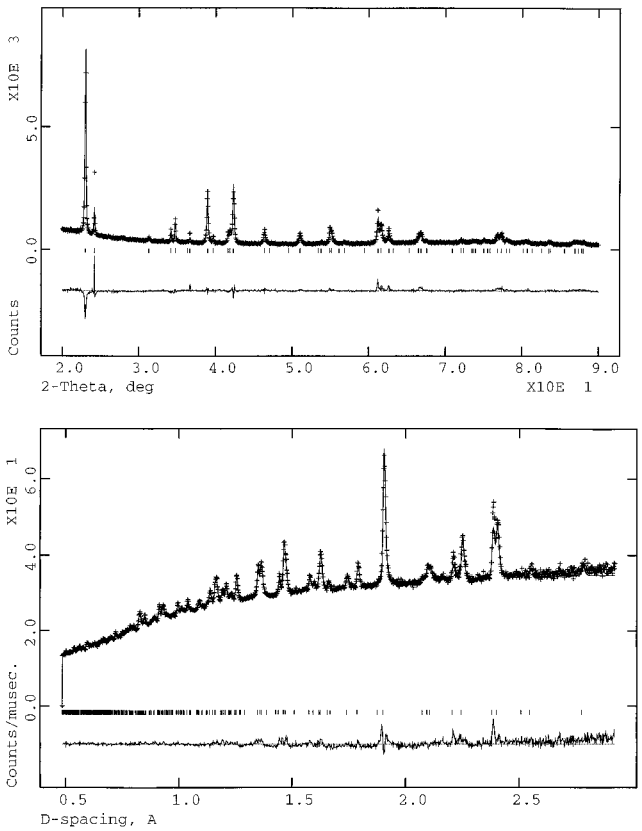

Figure 3. (a, top) Final Rietveld fit for (**1**): crosses represent observed data (X-ray data), the solid line is the calculated pattern, and the difference profile and allowed reflection positions are shown beneath. (b, bottom) Final Rietveld fit for **1**: crosses represent observed data (neutron data), the solid line is the calculated pattern and the difference profile and allowed reflection positions are shown beneath.

The view of the unit cell of **1** is shown in Figure 6. Final atomic positional and thermal parameters are given in Table 2 with a summary of the important bond distances and angles listed in Table 6.

Analysis of the X-ray powder patterns of both **2** and **3** indicated that they could be indexed on similar hexagonal unit cells of $a = 5.09$ and $c = 14.9$ Å for **2** and $a = 5.1$ and $c = 14.4$ Å. for **3**. Rietveld refinements for both these materials were carried out starting from the initial solution found for **1**. For **3** the nitrate ions

Table 2. Fractional Atomic Coordinates and Occupancies for 1 (Esd's in Parentheses)

atom	site	x	y	z	occupancy
Al	4d	1/3	2/3	0	1.0
O	12k	0.6350(2)	0.6350(2)	0.56720(7)	1.0
H	12k	0.6879(5)	0.6879(5)	0.6335(1)	1.0
Cl	2a	0	0	1/4	1.0
Li	2b	0	0	0	1.0

Table 3. Fractional Atomic Coordinates and Occupancies for 2 (Esd's in Parentheses)

atom	site	x	y	z	occupancy
Al	4d	1/3	2/3	0	1.0
O	12k	0.6355(6)	0.6355(6)	0.5636(2)	1.0
Br	2a	0	0	1/4	1.0
Li	2b	0	0	0	1.0

Table 4. Fractional Atomic Coordinates and Occupancies for 3 (Esd's in Parentheses)

atom	site	x	y	z	occupancy
Al(1)	4f	1/3	2/3	0	1.0
O(1)	12i	0.6361(9)	0.6401(9)	0.5717(1)	1.0
N(1)	2a	0	0	1/4	1.0
O(2)	6h	0.734(1)	0.797(1)	1/4	0.847(8)
O(3)	6h	0.266(1)	0.203(1)	1/4	0.153(8)
Li(1)	2b	0	0	0	1.0

intercalated between the $Al(OH)_3$ layers were found to be disordered. In both arrangements of the nitrate ion the nitrogen atoms coordinates remained invariant and the coordinates of O(2) and O(3) were refined using the constraints: [x(O(2)) = −x{O(3)}, y{O(2)} = −y{O(3)}, Occup{O(2)} + Occup{O(3)} = 1]. This model generates two disordered nitrate ions which are related by a 180° rotation in the crystallographic *ab* plane. The final X-ray data refinement of **2** consisted of 29 parameters with 3101 data points (37 reflections) and 32 parameters with 4100 data points (104 reflections) for **3**. An overall isotropic thermal parameter, $B = 0.66(3)$ and 0.42(2) Å^2 was used for **2** and **3**, respectively. Final convergence was achieved at $\chi^2 = 6.18$, 5.99, $R_{wp} = 6.39\%$, 6.77% for **2** and **3**, respectively. A full summary of the crystallographic details for both **2** and **3** is given in Table 1. Tables 3 and 4 give the final atomic positions and thermal parameters of **2** and **3**, respectively. A plot of the final Reitveld fits of the powder X-ray data for **3** is shown in Figure 4. A summary of the chemically important bond lengths and angles is given in Table 6.

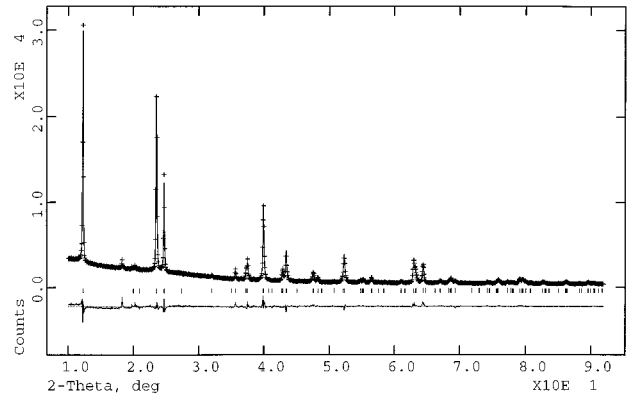

Figure 4. Final Rietveld fit for **3**: crosses represent observed data (X-ray data), the solid line is the calculated pattern, and the difference profile and allowed reflection positions are shown beneath.

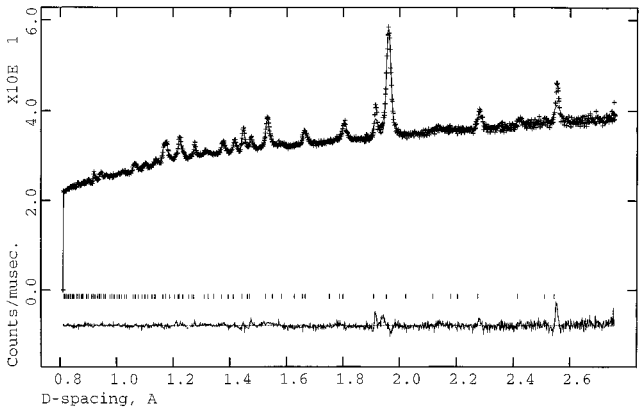

Figure 5. Final Rietveld fit for **4**: crosses represent observed data (neutron data), the solid line is the calculated pattern, and the difference profile and allowed reflection positions are shown beneath.

Table 5. Fractional Atomic Co-Ordinates and Occupancies for 4 (Esd's Are Given in Parentheses)

atom	site	*x*	*y*	*z*	occupancy
Al(1)	4f	$^1/_3$	$^2/_3$	0	1.0
O(1)	12i	0.6424(9)	0.644(1)	0.5631(1)	1.0
H(11)	12i	0.693(2)	0.658(2)	0.629(2)	1.0
Li(1)	2b	0	0	0	1.0
Cl(1)	6h	0.35(1)	0.35(1)	$^1/_4$	0.0667
Cl(2)	6h	0.191(9)	0.63(1)	$^1/_4$	0.0667
Cl(3)	6h	0.63(1)	0.191(9)	$^1/_4$	0.0667
Cl(4)	6h	0.08(1)	0.24(1)	$^1/_4$	0.0667
Cl(5)	6h	0.242(7)	0.08(1)	$^1/_4$	0.0667
O(2)	6h	0.388(7)	0.263(9)	$^1/_4$	0.0733
O(3)	6h	0.163(7)	0.505(9)	$^1/_4$	0.0733
O(4)	6h	0.629(7)	0.04(9)	$^1/_4$	0.0733
O(5)	6h	0.053(7)	0.118(9)	$^1/_4$	0.0733
O(6)	6h	0.242(7)	−0.071(9)	$^1/_4$	0.0733
H(1)	6h	0.23(2)	0.003(9)	$^1/_4$	0.0733
H(2)	6h	0.574(2)	0.30(2)	$^1/_4$	0.0733
H(3)	6h	0.01(2)	0.245(9)	$^1/_4$	0.0733
H(4)	6h	0.351(9)	0.54(1)	$^1/_4$	0.0733
H(5)	6h	0.51(1)	0.12(1)	$^1/_4$	0.0733
H(6)	6h	0.87(1)	0.24(1)	$^1/_4$	0.0733
H(7)	6h	−0.10(2)	−0.143(9)	$^1/_4$	0.0733
H(8)	6h	0.238(9)	0.15(1)	$^1/_4$	0.0733
H(9)	6h	0.12(1)	0.011(1)	$^1/_4$	0.0733
H(10)	6h	0.49(1)	0.13(1)	$^1/_4$	0.0733

In the case of the hydrated phase $[LiAl_2(OH)_6]Cl{\cdot}H_2O$ (**4**), the X-ray and neutron diffraction patterns were of significantly poorer quality compared to compounds **1**−**3**, indicating an increase in the crystallographic disorder on hydration. The unit cell of **4** appeared to be extrememly sensitive to the degree of hydration, the age of the sample and the humidity of the atmosphere in which it was stored. Therefore we were unable to carry out simultaneous X-ray and neutron powder refinements on the two room-temperature data sets that we collected. The powder neutron data was of higher quality, and so we discuss the refinement of the structure using solely these data. The powder neutron diffractograms of **4** could be indexed on a slightly enlarged hexagonal unit cell of dimensions $a = 5.1$ and $c = 15.3$ Å. Starting with the two $Al(OH)_3$ layer structural model found for compounds **1**−**3**, we computed a Fourier map midway between the $Al(OH)_3$ layers, i.e., in the $z = 0.25$ plane. This map showed that the chlorine and oxygens atoms were positionally disordered over a number of sites. We were able to successfully model this disorder by allowing the chlorine and oxygen atoms to occupy five sites in the $z = 0.25$ plane. Refinement of the occupancy of oxygen over these five possible sites gave a total oxygen occupancy of 0.98, which is in excellent agreement with the chemical analysis. The hydrogens on the oxygen atoms were allowed to ride on their attached oxygens at a fixed O−H bond length of 1.0 Å. An overall isotropic thermal parameter, $B = 0.49(2)$ Å^2 was used. The final neutron data refinement of **4** consisted of 51 parameters, with 3585 data points (291 reflections). Final convergence was achieved at $\chi^2 = 5.27$, $R_{wp} = 1.26$. A full summary of the crystallographic details for **4** is given in Table 1. A plot of the final Rietveld fits of the powder neutron data for **4** is shown in Figure 5.

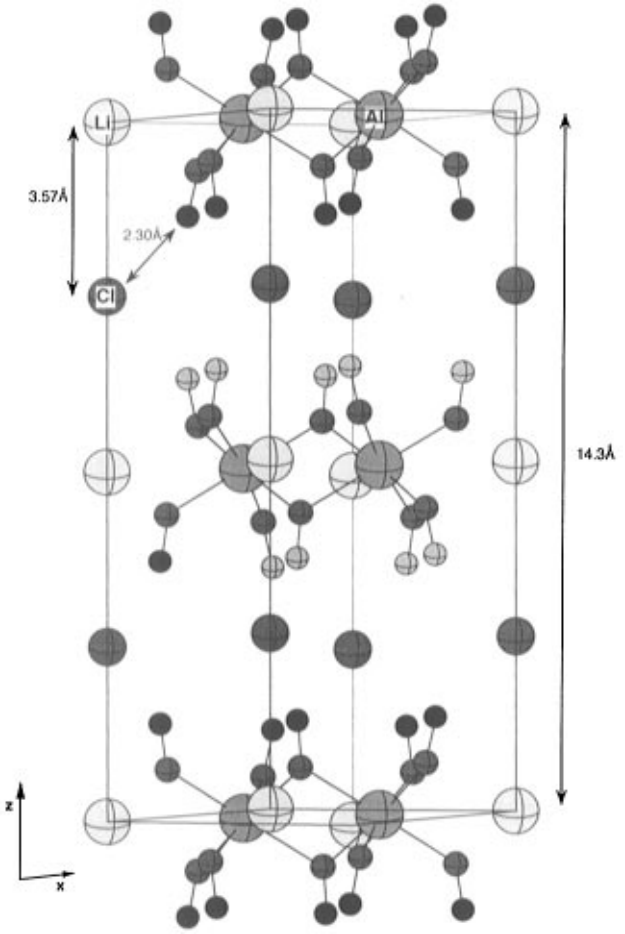

Figure 6. View of the unit cell of **1** showing some of the chemically important distances.

Table 6. Summary of Selected Interatomic Distances and Angles in Compounds 1−4

bond length/Å and angles/deg	compound 1	2	3	4	gibbsite
	distances: Al ($^1/_3$,$^2/_3$,0)				
Al−Al1 ($-^1/_3$,$^1/_3$,0)	2.94449(4)	2.94427(6)	2.94977(5)	2.9424(2)	
Al−Al2 ($^2/_3$,$^1/_3$,0)	2.94449(4)	2.94428(6)	2.94978(5)	2.9424(2)	
Al−Al3 ($^2/_3$,$^4/_3$,0)	2.94449(4)	2.94427(6)	2.94977(5)	2.9424(2)	
Al−Li1 (0,0,0)	2.94449(4)	2.94428(6)	2.94978(5)	2.9424(2)	
Al−Li2 (0,1,0)	2.94449(4)	2.94427(6)	2.94977(5)	2.9424(2)	
Al−Li3 (1,1,0)	2.94449(4)	2.94428(6)	2.94978(5)	2.9424(2)	
	AlO_6 Octahedra: Al ($^1/_3$,$^2/_3$,0)				
Al−O1 (0,0.6350,0.0672)	1.8881(7)	1.883(2)	1.946(5)	1.911(5)	1.862
Al−O2 (0.3650,0.3650,0.0672)	1.8882(7)	1.883(2)	1.946(5)	1.911(5))	1.930
Al−O3 (0.6350,1.0000,0.0672)	1.8881(7)	1.883(2)	1.946(5)	1.911(5)	1.881
Al−O4 (0,0.3650,−0.0672)	1.8881(7)	1.883(2)	1.920(5)	1.898(4)	1.947
Al−O5 (0.6350,0.6350,−0.0672)	1.8882(7)	1.883(2)	1.920(5)	1.898(4)	1.922
Al−O6 (0.3650,1.0000,−0.0672)	1.8881(7)	1.883(2)	1.920(5)	1.898(4)	1.890
O1−Al−O2,O1−Al−O3,O2−Al−O3	96.40(4)	96.8(1)	94.5(1)	96.1(2)	
O4−Al−O5,O4−Al−O6,O5−Al−O6	96.40(4)	96.8(1)	93.9(1)	96.5(2)	
O1−Al−O4,O2−Al−O5,O3−Al−O6	77.53(5)	77.2(1)	80.54(9)	79.4(1)	
O1−Al−O5,O2−Al−O6,O3−Al−O4	171.51(6)	171.6(2)	172.5(2)	174.1(2)	
O2−Al−O4,O1−Al−O6,O3−Al−O5	90.22(7)	89.8(2)	91.5(2	88.3(2)	
	LiO_6 Octahedra: Li (0,0,0)				
Li−O1 (0,−0.3650,0.0672)	2.095(1)	2.088(3)	2.117(3)	2.057(3)	
Li−O2 (0.3650,0.3650,0.0672)	2.095(1)	2.088(3)	2.117(3)	2.057(3)	
Li−O3 (−0.3650,0,0.0672)	2.095(1)	2.088(3)	2.117(3)	2.057(3)	
Li−O4 (0,0.3650,−0.0672)	2.095(1)	2.088(3)	2.117(3)	2.057(3)	
Li−O5 (−0.3650,−0.3650,−0.0672)	2.095(1)	2.088(3)	2.117(3)	2.057(3)	
Li−O6 (0.3650,0,−0.0672)	2.095(1)	2.088(3)	2.117(3)	2.057(3)	
O1−Li−O2,O1−Li−O3,O2−Li−O3	100.62(4)	100.91(9)	98.30(7)	99.37(9)	
O4−Li−O5,O4−Li−O6,O5−Li−O6	100.62(4)	100.91(9)	98.30(7)	99.37(9)	
O1−Li−O4,O3−Li−O6	179.960	180.000	179.960	180.000	
O2−Li−O5	180.000	179.960	179.960	180.00	
O1−Li−O5,O1−Li−O6,O2−Li−O4	79.38(4)	79.09(9)	81.70(7)	80.63(9)	
O2−Li−O6,O3−Li−O4,O3−Li−O5	79.38(4)	79.09(9)	81.70(7)	80.23(9)	

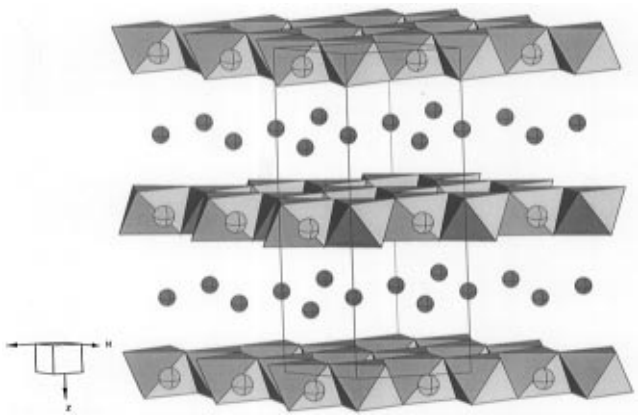

Figure 7. View of the structure of **1** showing the $Al(OH)_3$ layer alternation.

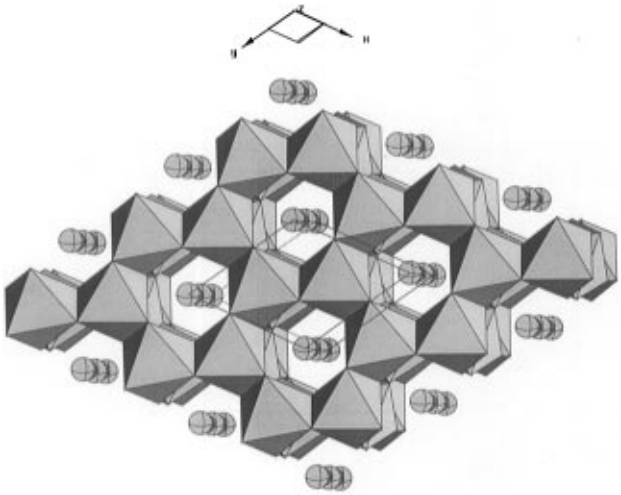

Figure 8. View down the [001] direction of the unit cell of **1**. Li^+ occupies empty octahedral holes in $Al(OH)_3$ layer and the Cl^- occupies the position midway between the layers to form a $Li^+\cdots Cl^-\cdots Li^+\cdots Cl^-$ chain.

Discussion of Structures. Since compounds **1** and **2** are isostructural and **3** has a very similar structure, we will discuss them together. A view of the unit cell of **1** is shown in Figure 6. Unusually, both the anion and cations are incorporated into the host lattice. The interlayer distance between the $Al(OH)_3$ layers increases by Δc = 2.3 Å (**1**), 2.63 Å (**2**), 2.34 Å (**3**), 2.8 Å (**4**) to accommodate the X^- ions (Figure 7). To maintain charge neutrality, the Li^+ ions are incorporated into the octahedral holes in the $Al(OH)_3$ layers. Very little structural changes are observed in the aluminum coordination; the Al is still in an almost ideal octahedral environment with average Al−O bond lengths of 1.8881(7), 1.883(2), and 1.933(5) Å for **1**−**3**, respectively. This represents almost no change from the average Al−O bond length of 1.905 Å found in the crystal structure determination of natural gibbsite. The closest Cl···H contact in **1** is 2.304(2) Å, which suggests that there are no significant hydrogen bonding interactions with Cl^- ions and −OH groups in the $Al(OH)_3$ layers. The Li^+ ions are also located in the octahedral site within the $Al(OH)_3$ layers the Li−O bond lengths vary from 2.095(1) Å for **1** to 2.117(3) Å for **3**.

Viewing the structure of **1**−**3** down the *c*-axis clearly shows the relative arrangements of the anions and cations. The Li^+ and X^- ions line up parallel to the *c*-axis and form an alternating $Li^+\cdots X^-\cdots Li^+\cdots$ chain as shown in Figure 8. Another interesting feature is the eclipsed $Al(OH)_3$ layers resulting in a 6 L structure

(aAXAaBXBa; a = metal layer, A, B = hydroxide layer, and X = anion layer).

In **4** the stacking arrangement of the $Al(OH)_3$ layers remains the same resulting in a 6 L structure; however. there is significantly more disorder between the $Al(OH)_3$ layers and there are still some discrepancies between the observed and calculated profiles. Fourier maps computed midway between the $Al(OH)_3$ layers show no evidence for localization of the oxygen or chlorine electron density on particular lattice sites. We have modeled this disorder by allowing the water and chloride ions to randomly distribute themselves over five possible interlayer sites. Another possibility is that in fact the Li and Al positions are ordered within each layer but are not in *c*-axis registry, we believe this is less likely since compounds **1**−**3** are well-ordered structures. Although there is extensive disorder between the $Al(OH)_3$ layers, we see no evidence for significant stacking fault disorder of the $Al(OH)_3$ layers along the *c*-axis. Poeppelmeier and co-workers have carried out a detailed study of $[LiAl_2(OH)_6]OH{\cdot}2H_2O$.[17] They conclude that in this material the disorder in the positions of the Li and Al atoms is caused not by intralayer positional disorder but by translational, interlayer disorder.

Conclusion

Gibbsite has been shown to intercalate a range of lithium salts. Both the lithium ions and the halide or nitrate counteranions are intercalated into the host structure. These materials readily dehydrate giving highly crystalline intercalates. The crystal structures of these materials show they are highly ordered lamellar phases consisting of eclipsed $[LiAl_2(OH)_6]^+$ layers sandwiching layers of intercalated anions.

Acknowledgment. We would like to thank the EPSRC for financial support and access to the ISIS (Rutherford Appleton Laboratory) and the SRS (Daresbury Laboratory). A.V.B also wishes to thank the Soros/FCO Scholarship Scheme for the award of a Visiting Studentship.

CM960316Z